Physics-informed neural networks for Richardson-Richards equation: Estimation of constitutive relationships and soil water flux density from volumetric water content measurements

Toshiyuki Bandai [1], Teamrat A. Ghezzehei [1]

[1]Life and Environmental Science Department, University of California, Merced, 5200, Lake Rd, Merced, CA, 95343, USA

Key Points:

- Water retention curve and hydraulic conductivity function were estimated from soil moisture dynamics using physics-informed neural networks.
- Soil water flux density was accurately derived from the trained physics-informed neural networks.
- The proposed framework was shown to be a promising inversion method to analyze soil moisture dynamics for practical field applications.

Corresponding author: Toshiyuki Bandai, `tbandai@ucmerced.edu`

Abstract

Water retention curve (WRC) and hydraulic conductivity function (HCF) are essential information to model the movement of water in the soil using the Richardson-Richards equation (RRE). Although laboratory measurement methods of WRC and HCF have been well established, the lab-based WRC and HCF can not be used to model soil moisture dynamics in the field because of the scale mismatch. Therefore, it is necessary to derive the inverse solution of the RRE and estimate WRC and HCF from field measurement data. We are proposing a physics-informed neural networks (PINNs) framework to obtain the inverse solution of the RRE and estimate WRC and HCF from only volumetric water content measurements. The PINNs was constructed using three feedforward neural networks, two of which were constrained to be monotonic functions to reflect the monotonicity of WRC and HCF. The PINNs was trained using noisy synthetic volumetric water content data derived from the simulation of soil moisture dynamics for three soils with distinct textures. The PINNs could reconstruct the true soil moisture dynamics from the noisy data. As for WRC, the PINN could not precisely determine the WRCs. However, it was shown that the PINNs could estimate the HCFs from only the noisy volumetric water content data without specifying initial and boundary conditions and assuming any information about the HCF (e.g., saturated hydraulic conductivity). Additionally, we showed that the PINNs framework could be used to estimate soil water flux density with a broader range of estimation than the currently available methods.

1 Introduction

Soil moisture data is vital for weather forecasting and hydrological modeling, managing agriculture and crop productivity, and predicting natural disasters, such as landslides and flood, and drought (Robinson et al., 2008; Babaeian et al., 2019). Notably, detailed information about near-surface soil moisture dynamics is essential for land surface modeling and remote sensing applications. Therefore, several measurement methods have been proposed to monitor the movement of water near the surface soil, such as a TDR array probe (Sheng et al., 2017) and heat pulse method (Kamai et al., 2008, 2010).

The dynamics of soil moisture can be expressed by the Richardson-Richards equation (RRE) (Richardson, 1922; Richards, 1931). The RRE is a non-linear partial differential equation (PDE) and has been extensively studied (Farthing & Ogden, 2017; Zha et al., 2019). The RRE is composed of the continuity equation and the Buckingham-Darcy's law (Buckingham, 1907). The RRE consists of three primary variables: matric potential ψ, volumetric water content θ, and hydraulic conductivity K. Volumetric water content and hydraulic conductivity are both functions of matric potential, which are referred to as water retention curve (WRC) and hydraulic conductivity function (HCF), respectively. These two soil hydraulic functions (also called constitutive relationships) embody the characteristic features of soil pore network and are the manifestation of the interactions between soil texture and structure. These constitutive relationships are necessary to solve the RRE and commonly expressed through parametric models (Brooks & Corey, 1964; van Genuchten, 1980; Durner, 1994; Kosugi, 1996).

Although laboratory methods for measuring WRC and HCF have been well established, lab-based WRC and HCF cannot be directly applied to modeling soil moisture dynamics in the field because of the scale mismatch between laboratory experiments and field measurements (Hopmans et al., 2002). Therefore, it is indispensable to estimate WRC and HCF using the inverse solution of the RRE from field data.

Many studies have attempted to determine the parameters of soil hydraulic functions, such as Mualem-van Genuchten model (van Genuchten, 1980) from synthetic or experimental data using a global optimization algorithm (Durner et al., 2008) or Gaussian processes (Rai & Tripathi, 2019). On the other hand, several studies employed free-form soil hydraulic functions to estimate WRC and HCF (Bitterlich et al., 2004; Iden & Durner, 2007). The advantage of the free-form approach over the parametric models is that (1) we do not need to assume soil hydraulic functions a priori, and (2) the error in WRC does not propagate into HCF, especially for near saturation by decoupling WRC and HCF rather than employing capillary bundle model (Mualem, 1976). However, these studies are based on the forward solution of the RRE and need initial and boundary conditions, which are not readily available in most practical situations.

In terms of the inverse solution of PDEs, a deep learning framework called physics-informed neural networks (PINNs) was proposed by Raissi et al. (2019). PINNs employs the universal approximation capability of neural networks (Cybenko, 1989) to approximate the solution of PDEs, and the parameters of the neural networks are trained by minimizing the sum of data-fitting error and the residual of the PDEs simultaneously. This simultaneous learning enables PINNs to learn the dynamics of the system from measurement data and physics. This PINNs approach has been successful in several fields of computational physics (Raissi & Karniadakis, 2018; Tartakovsky et al., 2018; Raissi et al., 2019; Wang et al., 2020). Particularly, Tartakovsky et al. (2018) employed PINNs to determine the hydraulic conductivity function of an unsaturated homogeneous soil from synthetic matric potential data based on the two-dimensional time-independent RRE.

In this paper, we are proposing a new framework for the inverse solution of the time-dependent RRE to estimate the constitutive relationships (both WRC and HCF) using PINNs with fewer assumptions than conventional inverse solution approaches. We emphasize that only volumetric water content was used as measurement data rather than matric potential data because the range and accuracy of matric potential measurements are still limited, though there have been recent advances (Degré et al., 2017). Additionally, we used monotonic neural networks (Daniels & Velikova, 2010) to employ the advantage of the free-formed approach of WRC and HCF (Bitterlich et al., 2004; Durner et al., 2008).

Here, the feasibility of the framework is tested using synthetic volumetric water content time-series data generated by HYDRUS-1D for three types of homogeneous soil (sandy loam, loam, and silt loam). The robustness of the method is evaluated by comparing the WRC and HCF estimated by the PINNs to the true ones. In addition, we show the potential of applying the fitted PINNs for estimating soil water flux density using only an array of soil moisture sensors.

2 Background

2.1 Richardson-Richards Equation

This subsection introduces the Richardson-Richards equation (RRE), which describes the movement of water in the saturated and unsaturated soil. In this study, we consider one-dimensional liquid water flow in the rigid soil and ignore water vapor, sink term, and histerisis. The mass balance of water in the soil leads to a continuity equation:

$$\frac{\partial \theta}{\partial t} = -\frac{\partial q}{\partial z}, \tag{1}$$

where θ is volumetric water content [$\mathrm{L}^3\ \mathrm{L}^{-3}$]; t is time [T]; z is vertical coordinate (positive upward) [L]; q is soil water flux density [L T^{-1}]. The soil water flux density q is related to matric potential of water in the soil ψ [L] through the Darcy-Buckingham's law (Buckingham, 1907):

$$q = -K\left(\frac{\partial \psi}{\partial z} + 1\right), \tag{2}$$

where K is hydraulic conductivity [L T^{-1}]. The two equations (Equation 1 and 2) are combined to derive the Richardson-Richards equation (RRE): (Richardson, 1922; Richards,

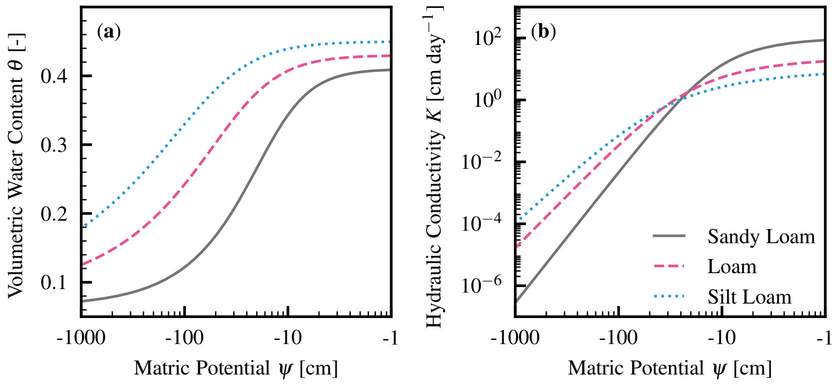

Figure 1: Constitutive relationships for three types of soil (sandy loam, loam, and silt loam) generated using Mualem-van Genuchen model (van Genuchten, 1980). (**a**) Water retention curves (WRC). (**b**) Hydraulic conductivity functions (HCF).

1931)

$$\frac{\partial \theta}{\partial t} = \frac{\partial}{\partial z}\left[K\left(\frac{\partial \psi}{\partial z}+1\right)\right]. \tag{3}$$

To solve the RRE, matric potential ψ is commonly treated as the dependent variable, and volumetric water content θ and hydraulic conductivity K are parameterized through matric potential ψ, as in

$$\frac{\partial \theta(\psi)}{\partial t} = \frac{\partial}{\partial z}\left[K(\psi)\left(\frac{\partial \psi}{\partial z}+1\right)\right]. \tag{4}$$

The functions $\theta(\psi)$ and $K(\psi)$ are called constitutive relationships and referred to as water retention curve (WRC) and hydraulic conductivity function (HCF) respectively. WRC and HCF are commonly expressed by parametric models (Brooks & Corey, 1964; van Genuchten, 1980; Durner, 1994; Kosugi, 1996). The WRCs and HCFs for three types of soil (sandy loam, loam, and silt loam soil) using Mualem-van Genuchen model (van Genuchten, 1980) are shown in Figure 1. As shown in the figure, both WRC and HCF are increasingly monotonic functions with respect to matric potential ψ. The monotonicity of WRC and HCF will be employed to design the architecture of neural networks in this study later on.

2.2 Feedforward Neural Networks

A standard feedforward neural network with three layers (1 hidden layer) is explained for the readers to understand the neural networks used in this study. The readers should refer to textbooks (e.g., Goodfellow et al. (2016)) for more general explanations.

Given a training dataset $\{\mathbf{x}^{(i)}, \mathbf{y}^{(i)}\}$, where superscript (i) denotes the ith training data; $\mathbf{x}^{(i)} \in \mathbb{R}^{n_x}$ is input vector for the size of the input n_x; $\mathbf{y}^{(i)} \in \mathbb{R}^{n_y}$ is output vector for the size of the output n_y, a neural network is a mathematical function mapping the input vector $\mathbf{x}^{(i)}$ to predicted output vector $\hat{\mathbf{y}}^{(i)} \in \mathbb{R}^{n_y}$:

$$\hat{\mathbf{y}}^{(i)} = \hat{f}(\mathbf{x}^{(i)}). \tag{5}$$

The hat operator represents prediction throughout the paper. The inside of the neural network $\hat{f}$ is often represented by layers of units (or neurons), as shown in Figure 2. Herein,

$\mathbf{a}^{[L]} \in \mathbb{R}^{n^{[L]}}$ denotes the vector value for the Lth layer of a neural network where the Lth layer is composed of $n^{[L]}$ units. Firstly, the input vector $\mathbf{x}^{(i)}$ is entered in the first layer:

$$\mathbf{a}^{[1]} = \mathbf{x}^{(i)}, \tag{6}$$

here $n^{[1]} = n_x$. Then, the value for the jth unit of the second layer $\mathbf{a}^{[2]}$ is calculated from all the units in the previous layer (i.e., the first layer) with the weight matrix $W^{[1]}$ and bias vector $b^{[1]}$ of the first layer in the following way:

$$a_j^{[2]} = g^{[1]} \left(\sum_{k=1}^{n^{[1]}} W_{j,k}^{[1]} a_k^{[1]} + b_j^{[1]} \right), \tag{7}$$

where $g^{[1]}$ is a non-linear activation function for the first layer, such as the hyperbolic tangent function (tanh) shown in Figure 2 (**b**). The jth unit of the third layer is computed from all the units of the second layer (hidden layer):

$$a_j^{[3]} = \sum_{k=1}^{n^{[2]}} W_{j,k}^{[2]} a_k^{[2]} + b_j^{[2]}. \tag{8}$$

Finally, the output vector $\hat{\mathbf{y}}^{(i)}$ is derived from the final layer with an output function h:

$$\hat{y}_j^{(i)} = h(a_j^{[3]}), \tag{9}$$

here $n^{[3]} = n_y$. In this study, the sigmoid function (Figure 2 (**c**)) and exponential function (Figure 2 (**d**)) are used for an output function.

The collection of the weight matrices $\mathbf{W} = \{W^{[1]}, W^{[2]}\}$ and bias vectors $\mathbf{b} = \{b^{[1]}, b^{[2]}\}$ are the parameters of the neural network, which are estimated by minimizing a loss function comprising of the output vector $\mathbf{y}^{(i)}$ (training data) and the predicted output vector $\hat{\mathbf{y}}^{(i)}$. The definition of the loss function varies depending on the purpose of the training.

It is well known that a feedforward neural network with more hidden layers has a better capability of function approximation (Goodfellow et al., 2016). A neural network with more than two hidden layers is called a deep neural network. In such a case, a hidden layer is computed from all the units of the previous hidden layer in the same way explained above (Equation 7).

In the next section, three feedforward neural networks are combined to construct physics-informed neural networks for the RRE, and the loss function for the PINNs framework will be defined to estimate WRC and HCF from volumetric water content measurements.

3 Methods

3.1 Physics-Informed Neural Networks for RRE

Physics-informed neural networks (PINNs) has been proposed as a deep learning framework to derive the forward and inverse solution of PDEs by Raissi et al. (2019). In this study, PINNs was used to derive the inverse solution of the RRE and the constitutive relationships (i.e., WRC and HCF) from a set of measured volumetric water content $\{t^{(i)}, z^{(i)}, \theta^{(i)}\}_{i=1}^{i=N}$, where N is the number of measurement data.

PINNs for the RRE was constructed using three feedforward neural networks as shown in Figure 3. The neural network (**a**) is a function mapping from time t and vertical coordinate z into predicted matric potential $\hat{\psi}$:

$$\hat{\psi}^{(i)} = \hat{f}_\psi(t^{(i)}, z^{(i)}; \mathbf{W}_\psi, \mathbf{b}_\psi), \tag{10}$$

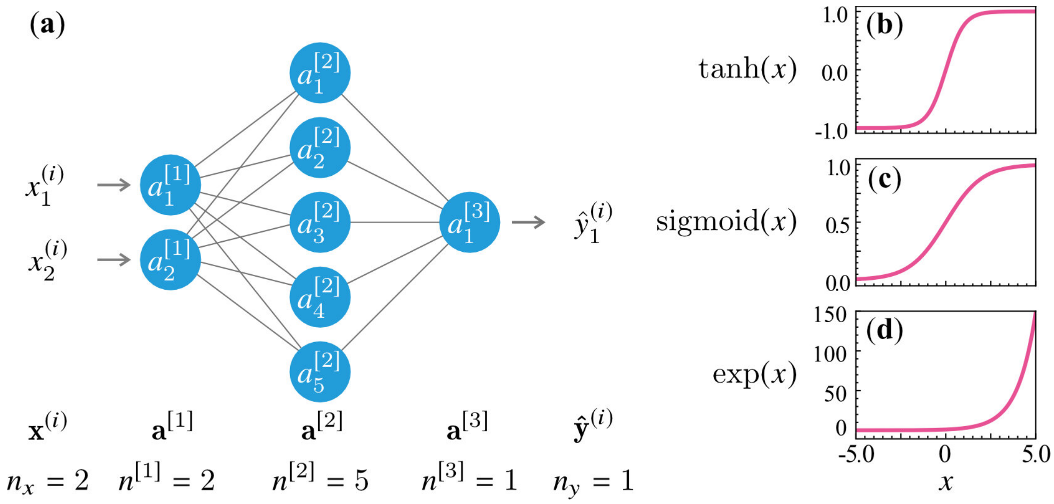

Figure 2: A feedforward neural network consisting of three layers with activation and output functions. (**a**) A feedforward neural network consisting of the input layer with two units, the hidden layer with five units, and the output layer with a one unit. (**b**) Hyperbolic tangent function. (**c**) Sigmoid function. (**d**) Exponential function.

where $\mathbf{W}_\psi$ and $\mathbf{b}_\psi$ are the collection of weight and bias parameters in the neural network. The hyperbolic tangent function (Figure 2 (**b**)) is used for the activation function as recommended in Raissi et al. (2019). The negative exponential function (i.e., $-\exp(x)$, see Figure 2 (**d**)) is used as the output function to force the predicted matric potential to be negative.

The predicted matric potential $\hat{\psi}$ is used to estimate volumetric water content $\hat{\theta}$ and hydraulic conductivity $\hat{K}$ through two distinct neural networks (Figure 3 (**c**) and (**b**) respectively). In other words, the two neural networks are employed to approximate the WRC and HCF for a given soil. Since WRC and HCF become simpler if matric potential is plotted in logarithmic scale, as in Figure 1, the predicted matric potential is converted into logarithmic scale by the following transformation:

$$\hat{\psi}_{\text{log}} = -\log_e(-\hat{\psi}). \tag{11}$$

The negative sign before the logarithm ensures WRC and HCF remain increasingly monotonic functions with respect to $\hat{\psi}$. Then, the predicted matric potential in logarithmic sclae $\hat{\psi}_{\text{log}}$ is used as the input value for the two neural networks:

$$\hat{\theta}^{(i)} = \hat{f}_\theta(\hat{\psi}^{(i)}_{\text{log}}; \mathbf{W}_\theta, \mathbf{b}_\theta), \tag{12}$$

$$\hat{K}^{(i)} = \hat{f}_K(\hat{\psi}^{(i)}_{\text{log}}; \mathbf{W}_K, \mathbf{b}_K). \tag{13}$$

The tanh function is used as the activation function for both neural networks. The output functions for $\hat{f}_\theta$ and $\hat{f}_K$ are the sigmoid function and exponential function respectively to ensure predicted volumetric water content between 0 and 1 and positive predicted hydraulic conductivity (see Figure 2 (**c**) and (**d**)).

To embrace the monotonicity of WRC and HCF, the weight parameters $\mathbf{W}_\psi$ and $\mathbf{W}_K$ are constrained to be non-negative so that $\hat{f}_\theta$ and $\hat{f}_K$ are increasingly monotonic functions with respect to the predicted matric potential $\hat{\psi}$ (Daniels & Velikova, 2010). The monotonicity honors the physical nature of WRC and HCF of all soils. This approach is similar to the free-form approach (Bitterlich et al., 2004; Iden & Durner, 2007), where

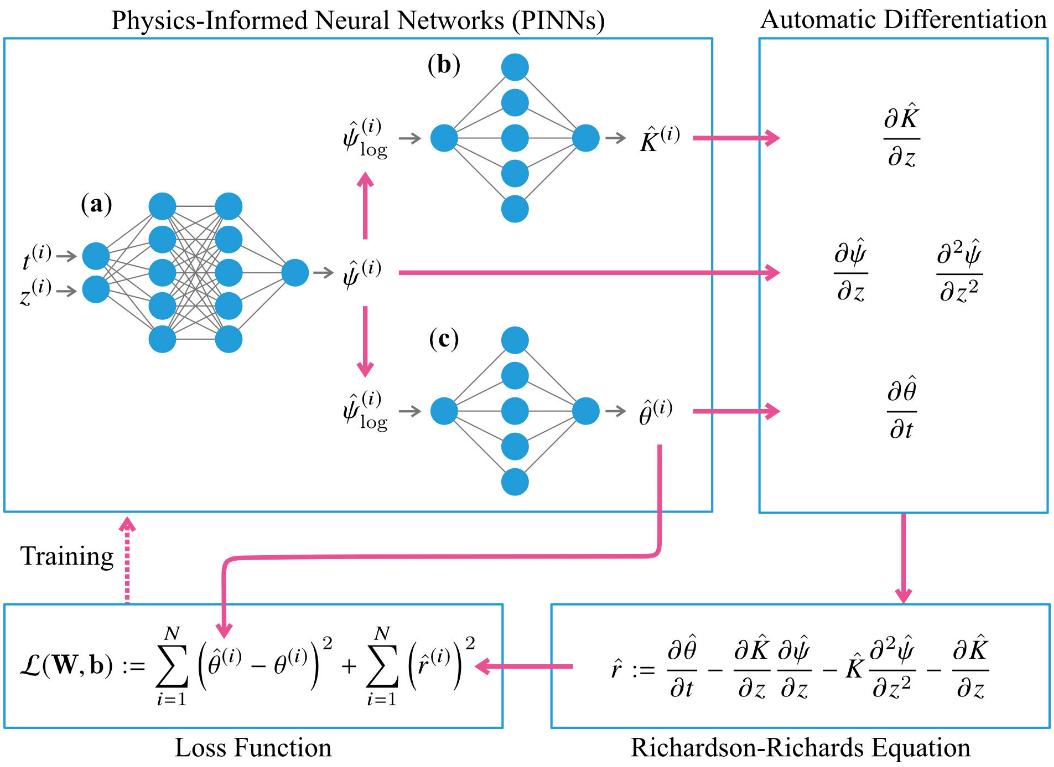

Figure 3: Physics-informed neural networks (PINNs) for the Richardson-Richards equation consisting of three feedforward neural networks to predict (**a**) matric potential $\hat{\psi}$ (10 hidden layers with 40 units), (**b**) volumetric water content $\hat{\theta}$ (1 hidden layer and 20 units), and (**c**) hydraulic conductivity $\hat{K}$ (1 hidden layer and 20 units). The number of layers and units in the figure is not actual.

cubic Hermite interpolation was used to approximate WRC and HCF. Unlike their studies, our monotonic neural network approach does not assume predetermined saturated water content and hydraulic conductivity, which are not easily available in the field application.

The collection of the parameters in the three neural networks $\mathbf{W} = \{\mathbf{W}_\psi, \mathbf{W}_\theta, \mathbf{W}_K\}$ and $\mathbf{b} = \{\mathbf{b}_\psi, \mathbf{b}_\theta, \mathbf{b}_K\}$ are identified by minimizing a loss function defined as

$$\mathcal{L}(\mathbf{W}, \mathbf{b}) := \sum_{i=1}^{N} (\hat{\theta}^{(i)} - \theta^{(i)})^2 + \sum_{i=1}^{N} (\hat{r}^{(i)})^2, \tag{14}$$

where $\hat{r}$ is the residual of the RRE defined as

$$\hat{r} := \frac{\partial \hat{\theta}}{\partial t} - \frac{\partial}{\partial z}\left[\hat{K}\left(\frac{\partial \hat{\psi}}{\partial z} + 1\right)\right] = \frac{\partial \hat{\theta}}{\partial t} - \frac{\partial \hat{K}}{\partial z}\frac{\partial \hat{\psi}}{\partial z} - \hat{K}\frac{\partial^2 \hat{\psi}}{\partial z^2} - \frac{\partial \hat{K}}{\partial z}. \tag{15}$$

The first term of the loss function (Equation 14) represents the fitting error of volumetric water content, and the second term represents the contraint by the RRE. This simultaneous learning enables the PINNs to learn the dynamics of water in the soil from both volumetric water content data and knowledge in soil physics (the RRE and the monotonicity of WRC and HCF).

To calculate the residual of the RRE $\hat{r}$ at data points, all the derivatives (i.e., $\frac{\partial \hat{\theta}}{\partial t}$, $\frac{\partial \hat{\psi}}{\partial z}$, $\frac{\partial^2 \hat{\psi}}{\partial z^2}$, $\frac{\partial \hat{K}}{\partial z}$) are evaluated at the data points using automatic differentiation (Nocedal & Wright, 2006). The parameters $\mathbf{W}$ and $\mathbf{b}$ are estimated by minimizing the loss function:

$$\min_{\mathbf{W}, \mathbf{b}} \mathcal{L}(\mathbf{W}, \mathbf{b}). \tag{16}$$

The optimization problem was solved by the L-BFGS-B algorithm (Byrd et al., 1995) given initial values of the parameters obtained through the Adam algorithm (Kingma & Ba, 2014). The minimization of the loss function with iterations of the two algorithms is provided in the Figure S1 in the supporting information. This PINNs framework for the RRE was implemented through TensorFlow (Abadi et al., 2015), and the source code is available on xxx (GitHub URL is shown here after acceptance).

3.2 Synthetic training data generated by HYDRUS-1D

To test the PINNs framework for the RRE, synthetic training data was generated through HYDRUS-1D (Šimůnek et al., 2013). Soil moisture dynamics in the 100 cm of homogeneous three types of soil (sandy loam, loam, and silt loam) were simulated for three days. In this simulation, the soil column is uniformly discretized at a 0.5 cm interval. The initial matric potential of -1000 cm was set for all the depths. The bottom boundary condition was Neumann boundary condition:

$$\frac{\partial \psi}{\partial z} = 0. \tag{17}$$

The upper boundary condition was set as the atmospheric upper boundary condition, where two different scenarios of time-dependent surface flux density were applied (see Table 1).

Three types of soil (sandy loam, loam, and silt loam) were tested with the same initial and boundary conditions explained above. Mualem-van Genuchen model was used to parameterize the WRCs and HCFs for these soils (van Genuchten, 1980):

$$\theta(\psi) = \theta_r + \frac{\theta_s - \theta_r}{(1 + (-\alpha\psi)^n)^m}, \tag{18}$$

$$K(\theta(\psi)) = K_s S_e^l (1 - (1 - S_e^{1/m})^m)^2, \tag{19}$$

Table 1: Two scenarios of surface water flux density [cm day^{-1}] (positive upward) were applied to generate synthetic training data using HYDRUS-1D (Šimůnek et al., 2013).

Time (day)	Scenario 1	Scenario 2
0.25	-10	-10
0.50	0	0
1.0	0.3	0.3
1.5	0	-5
2.0	0.3	0.3
2.25	-10	-5
2.5	0	-5
3.0	0.3	0.3

Table 2: Mualem-van Genuchen fitting parameters for three types of soils (van Genuchten, 1980).

Parameters	Sandy Loam	Loam	Silt Loam
θ_r	0.065	0.078	0.067
θ_s	0.41	0.43	0.45
α	0.075	0.036	0.02
n	1.89	1.56	1.41
K_s [cm day^{-1}]	106.1	24.96	10.8
l	0.5	0.5	0.5

where θ_r, θ_s, α, n, K_s, and l are the fitting parameters; $m = 1 - 1/n$; and the effective saturation S_e is defined as

$$S_e = \frac{\theta - \theta_r}{\theta_s - \theta_r}. \tag{20}$$

The Maulem-van Genuchen fitting parameters for the three soils are summarized in Table 2.

As the training data for the PINNs, volumetric water content was sampled every 0.012 day (i.e., 251 data points for a depth) at 10 equally spaced different depths within the top of the 20 cm of the soil column (z = -1, -3, -5, -7, -9, -11, -13, -15, -17, -19 cm). To consider the measurement error in volumetric water content, Gaussian noise with the mean of zero and the standard deviation of 0.005 was added to the sampled volumetric water content, and the noisy data was used to train the PINNs. This amount of noise is comparable to the noise observed when volumetric water content is measured by the TDR technique (Skierucha, 2000). The effect of the noise is shown in Table S1 in the supporting information. The noisy volumetric water content at three depths ($z = -1, -9, -17$ cm) for sandy loam soil for the two scenarios are shown in Figure 4. Before discussing the results of the training of the PINNs using the noisy data, the architecture of the neural networks in the PINNs was determined by noise-free volumetric water content data, which is explained in the next section.

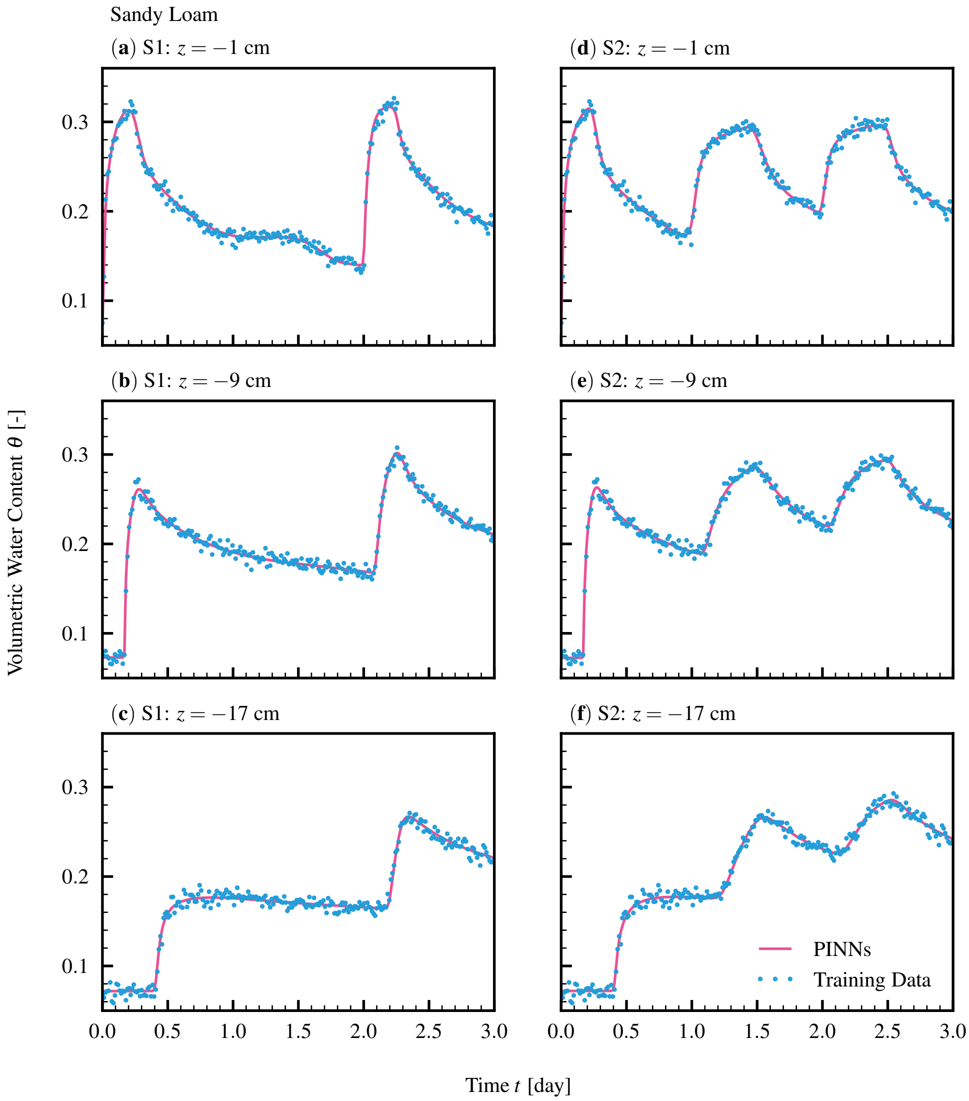

Figure 4: Predicted volumetric water content (PINNs) and noisy synthetic training data (Training Data) for sandy loam soil for the two scenarios at three different depths. Scenario 1 (S1): (**a**) $z = -1$ cm, (**b**) $z = -9$ cm, and (**c**) $z = -17$ cm. Scenario 2 (S2): (**d**) $z = -1$ cm, (**e**) $z = -9$ cm, and (**f**) $z = -17$ cm.

Table 3: The coefficient of determination R^2 between predicted volumetric water content and the synthetic training data with zero noise (Scenario 1) for silt loam soil and for different number of hidden layers and units for each hidden layer of the neural network for predicted matric potential (Figure 3 (**a**)).

	Units		
Hidden Layers	10	20	40
2	0.7909	0.9734	0.9777
4	0.9622	0.9865	0.9974
6	0.9930	0.9977	0.9988
8	0.9944	0.9978	0.9984
9	0.9975	0.9993	0.9992
10	0.9939	0.9990	0.9994
11	0.9970	0.9993	0.9991

3.3 Determination of the architecture of neural networks

The number of hidden layers and units for each hidden layer of the neural network for predicted matric potential $\hat{\psi}$ (Figure 3 (**a**)) was determined to be 10 hidden layers with 40 units for each hidden layer based on the coefficient of determination R^2 between volumetric water content predicted by the PINNs and the synthetic training data with zero noise generated by Scenario 1 (Table 1). The result of the investigation for silt loam soil is shown in Table 3, where seven different numbers of hidden layers and three different numbers of units for each layer were tested. The results for the other two soils are provided in Table S2 and S3 in the supporting information.

During the investigations, the neural networks for hydraulic conductivity and volumetric water content ((**b**) and (**c**) in Figure 3) were both set to have a one hidden layer consisting of 20 units. The effect of the number of the units of the hidden layer are provided in Table S4, S5, and S6 in the supporting information.

It should be noted that the results of the training were affected by the initial values of the parameters of the neural networks determined by Xavier initialization, as reported by Tartakovsky et al. (2018). Therefore, random seeds were carefully set in the algorithm to ensure the reproducibility of the results.

4 Results and Discussions

4.1 Soil Moisture Dynamics

The framework of PINNs for the RRE was tested with noisy synthetic volumetric water content data generated by HYDRUS-1D. Figure 4 shows predicted volumetric water content by the PINNs from noisy training data for sandy loam soil for the two scenarios. The PINNs could precisely capture the trend, including the sharp wetting fronts even though the training data was collapsed due to the noise. The PINNs could capture the trend well for the other two soils as well (shown in Figure S2 and S3 in the supporting information).

The PINNs could estimate the true volumetric water content without noise simulated by HYDRUS-1D from the noisy data, as shown in Figure 5. Larger errors were observed at the top of the sensor ($z = -1$ cm) and just after the initial condition. These were caused by the abrupt change in volumetric water content by infiltration. Sandy loam

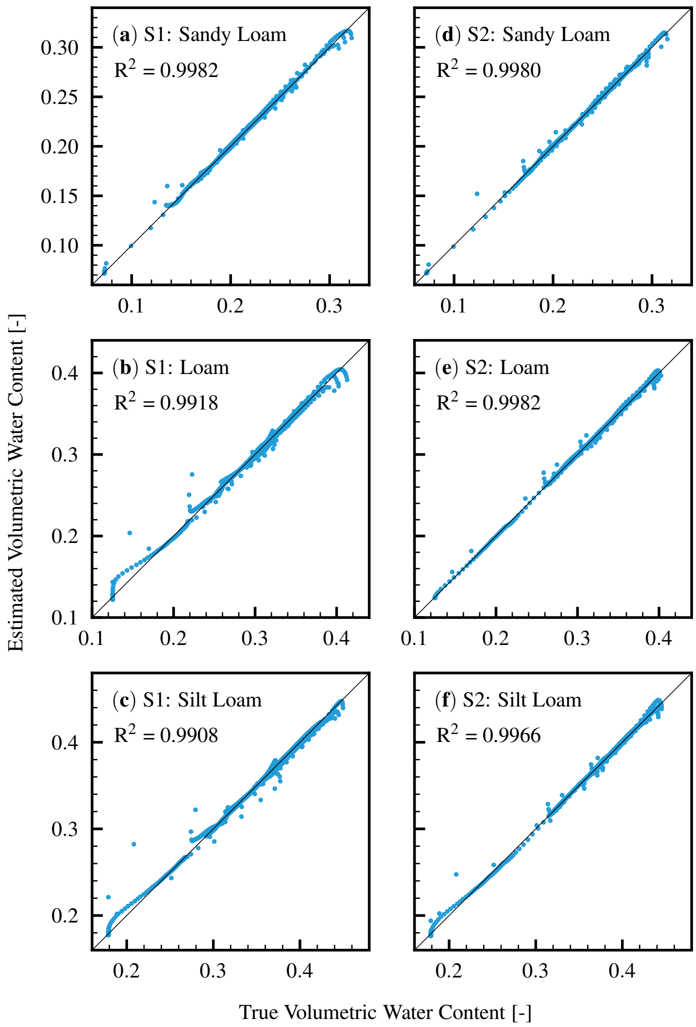

Figure 5: Comparison of the true volumetric water content with zero noise simulated by HYDRUS-1D to volumetric water content estimated by PINNs for the three soils and the two scenarios. Scenario 1 (S1): (**a**) sandy loam, (**b**) loam, and (**c**) silt loam. Scenario 2 (S2): (**d**) sandy loam, (**e**) loam, and (**f**) silt loam.

has higher R^2 values than loam and silt loam soils. Also, higher R^2 values were observed for Scenario 2 for all three soils, where more infiltration was applied to the top of the soil column. These two observations implied that more fluctuations within a given range of volumetric water content help PINNs to learn the soil moisture dynamics (see Figure 4).

The PINNs minimizes the data fitting error, as well as the residual of the RRE defined by Equation 15. The residual of the RRE for sandy loam soil at three different depths for the two scenarios is shown in Figure 6. Deviations from zero were observed at the time when infiltration reached the sensors. However, the values were distributed around zero, which means the RRE was satisfied at the sensor locations. Smaller deviations from zero were observed for sandy loam soil and Scenario 2, which correspond to the error in volumetric water content, as mentioned above. The results for the other soils are provided in Figure S4 and S5 in the supporting information.

4.2 Estimation of Constitutive Relationships

4.2.1 Water Retention Curve

The primary goal of the study was to predict soil hydraulic functions or constitutive relationships of the RRE (i.e., WRC and HCF). In terms of WRC, the PINNs could not precisely predict the WRCs for the three soils, as shown in Figure 7. Especially, the prediction was poor for low and high volumetric water content, where the training data points were not provided. Nevertheless, the predicted WRC for sandy loam soil for Scenario 2 was surprisingly similar to the true WRC regardless of the fact any actual value of matric potential was not used to train the PINNs.

How does the PINNs learn WRC from only volumetric water content? One possible explanation is that matric potential is estimated from the gradient of matric potential $\partial\hat{\psi}/\partial z$, which is calculated in the residual of the RRE $\hat{r}$. However, we still do not have a solid explanation for the learning mechanism of WRC and can not conclude the PINNs has the ability to predict WRC from only volumetric water content measurements. It should be noted that WRC must be flat near saturation, though this could not be reproduced by the PINNs. This mismatch must be improved in the near future research.

4.2.2 Hydraulic Conductivity Function

The estimated HCFs for the three soils for the two scenarios are shown in Figure 8. It should be noted that hydraulic conductivity is plotted against volumetric water content, not matric potential, as in Figure 1, because the estimated values of matric potential does not match the actual value, unlike volumetric water content.

The PINNs could estimate the HCFs, especially for sandy loam soil for Scenario 2, where high fluctuations in volumetric water content were observed (see Figure 4). Although there were errors in the estimation for a range of volumetric water content where few data points were used to train the PINNs, the estimation was fairly satisfactory for the middle range of volumetric water content.

Hydraulic conductivity was estimated probably through minimizing the residual of the RRE, which contains hydraulic conductivity (see Equation 15). Tartakovsky et al. (2018) reported that HCF could be estimated from matric potential measurements using PINNs with the time-independent RRE. Considering our result and their findings, hydraulic conductivity can be estimated from only each of volumetric water content and matric potential.

The advantage of the PINNs approach over the other studies to estimate HCF was that we did not assume any information about HCF a priori, such as saturated water

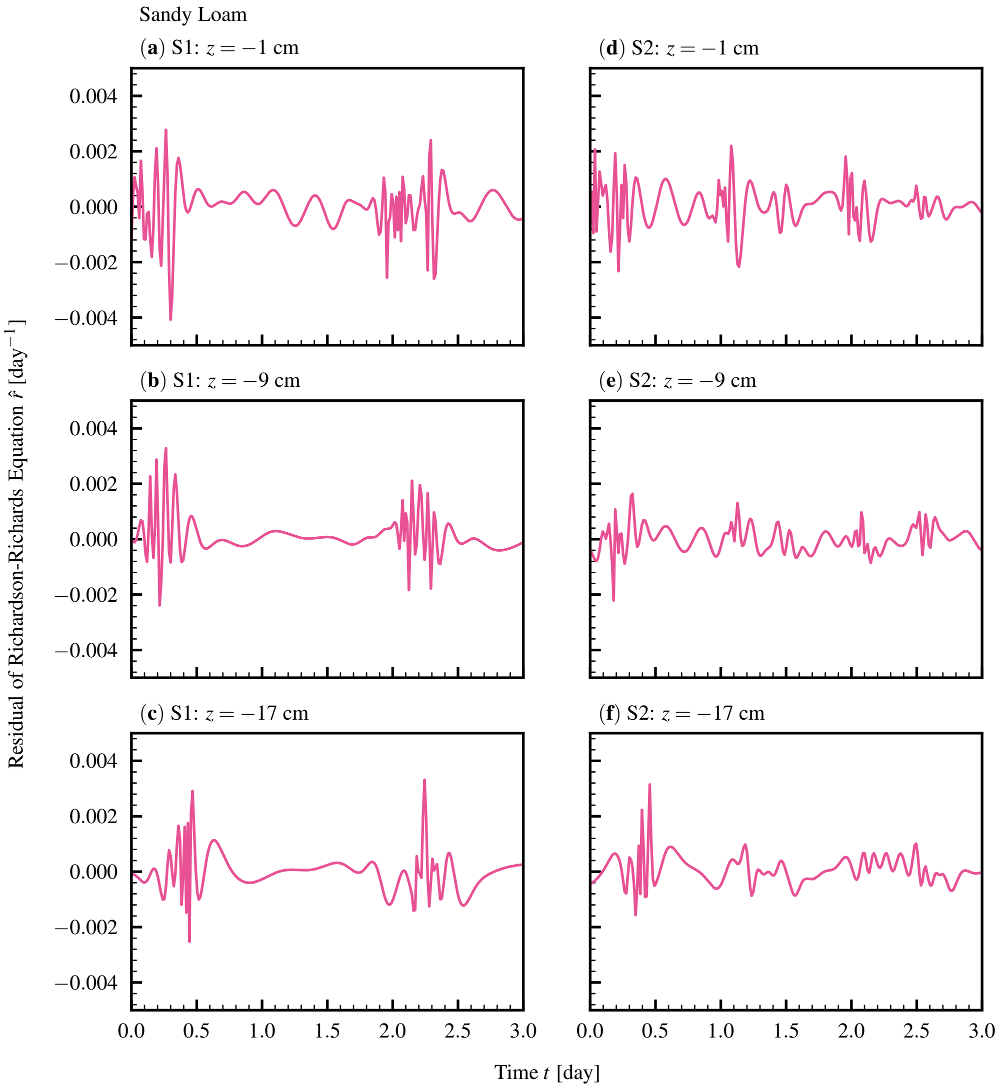

Figure 6: The residuals of the Richardson-Richards equation at three different depths for sandy loam soil for the two scenarios. Scenario 1 (S1): (**a**) $z = -1$ cm, (**b**) $z = -9$ cm, and (**c**) $z = -17$ cm. Scenario 2 (S2): (**d**) $z = -1$ cm, (**e**) $z = -9$ cm, and (**f**) $z = -17$ cm.

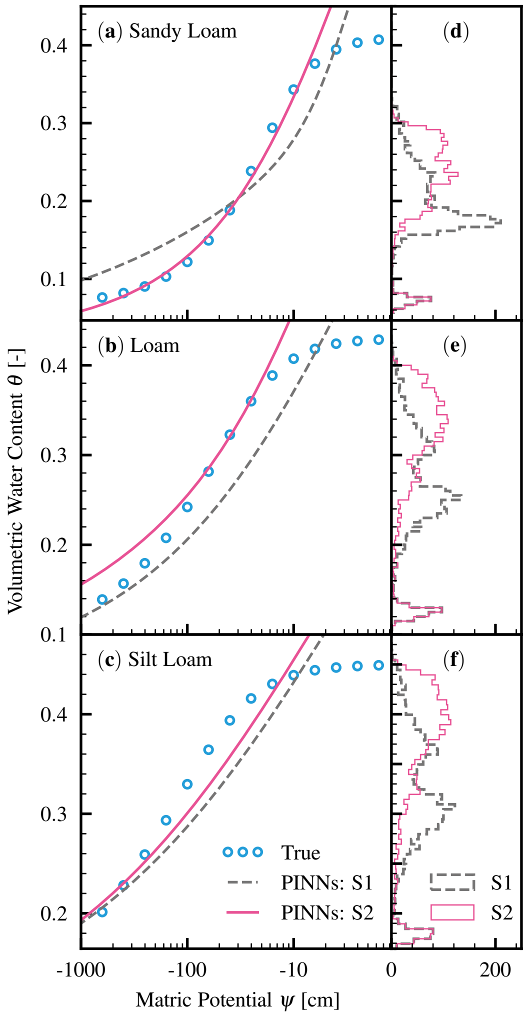

Figure 7: Comparison of true water retention curve (True) to the one predicted by the PINNs for the three soils for the two scenarios (S1: Scenario 1, S2: Scenario 2) with the histogram of the noisy training data. Water retention curve for (**a**) sandy loam, (**b**) loam, and (**c**) silt loam. Histogram of the training data for (**d**) sandy loam, (**e**) loam, and (**f**) silt loam.

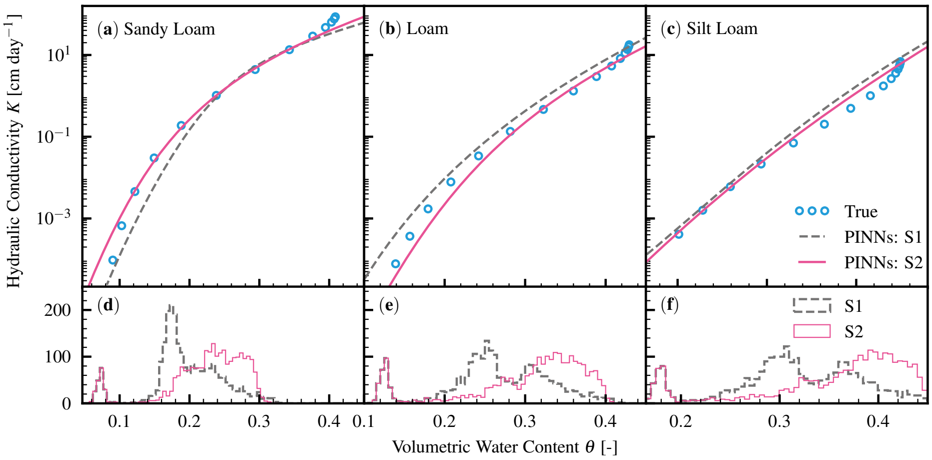

Figure 8: Comparison of true hydraulic conductivity function (True) to the one predicted by the PINNs for the three soils for the two scenarios (S1: Scenario 1, S2: Scenario 2) with the histogram of the noisy training data. Hydraulic conductivity function for (**a**) sandy loam, (**b**) loam, and (**c**) silt loam. Histogram of the training data for (**d**) sandy loam, (**e**) loam, and (**f**) silt loam.

content and saturated hydraulic conductivity. Also, the neural network for HCF is separated from WRC, which prevents the error in WRC from propagating into HCF. Considering these advantages, we conclude that the current framework of PINNs for the RRE is a powerful way to estimate HCF from only volumetric water content data, which has never been attained to the best of our knowledge.

4.3 Estimation of Soil Water Flux Density

In this section, we will show that the current PINNs framework can be used to estimate soil water flux density from noisy volumetric water content data. Soil water flux density was derived using the Buckingham-Darcy's law (Equation 2) with the estimated hydraulic conductivity $\hat{K}$, the gradient of the predicted hydraulic conductivity $\partial\hat{K}/\partial z$ and matric potential $\partial\hat{\psi}/\partial z$.

The comparison of the estimated soil water flux density to the true one calculated by HYDRUS-1D at three different depths ($z = -1, -9, -17$ cm) for the three soils for the two scenarios is shown in Figure 9, 10, and 11. It was found that the PINNs could estimate soil water flux density from noisy volumetric water content measurements. The predictive ability was associated with the accuracy of the estimation of volumetric water content and HCF, which is shown by the precise estimation of soil water flux density for sandy loam soil for Scenario 2 ($\mathrm{R}^2 = 0.9905$). Larger errors were observed at wetting fronts and the sensor located near the surface (i.e., $z = -1$cm), where soil water flux density changed abruptly. Although larger error was observed for loam and silt loam, especially for Scenario 1, the PINNs could reasonably capture the trend of soil water flux density by compensating the overestimation at some time for the underestimation at other time. Figure S6 in the supporting information summarizes the predictive ability of soil water flux density for all three soils.

The advantage of this approach over the available heat pulse method (Kamai et al., 2008, 2010) is that this method can estimate soil water flux density lower than 1 cm day^{-1} (see Figure S7, S8, and S9 in the supporting information). Because continuous measurement of volumetric water content at different depths is becoming popular with an advanced TDR array (Sheng et al., 2017), this PINNs approach can be used to estimate soil water flux density in the field. This finding has a significant implication in the application of land surface modeling, where soil water flux density near the surface is critical.

5 Conclusions

A framework of estimating soil hydraulic functions or constitutive relationships of the Richardson-Richards equation (RRE) (i.e., water retention curve (WRC) and hydraulic conductivity function (HCF)) from noisy volumetric water content measurements was proposed using physics-informed neural networks (PINNs). PINNs for the RRE was designed by endowing the neural networks with the monotonicity of WRC and HCF. To test this framework, synthetic volumetric water content data with noise simulated for three types of soil (sandy loam, loam, and silt loam) were used to train the PINNs, and the WRC, HCF, and soil water flux density were estimated.

The PINNs could estimate true soil moisture dynamics from noisy synthetic data for all types of soil. It was found that data with more fluctuations appear to help the PINNs to learn the soil moisture dynamics. In terms of WRC, the PINNs could not precisely estimate the true WRCs. However, the estimated WRC for sandy loam soil was similar to the true one regardless of the fact that any matric potential data was provided. Unlike WRC, the PINNs could predict the HCFs well, especially for sandy loam soil. The discrepancies of the estimated and actual HCFs were more significant for loam and silt loam soils than sandy loam soil, which could be explained by the magnitude of the fluctuations of the training data within the observed range.

The PINNs could estimate true soil water flux density from noisy synthetic volumetric water content data at different depths. At present, the only measurement technique for measuring soil water flux density is using heat flux sensors, which is limited to soil water flux density larger than 1 cm day^{-1}. The proposed method has the potential for determining soil water flux density over a broader range.

It was illustrated that the PINNs has a great potential to predict constitutive relationships of the RRE and soil water flux density from only noisy volumetric water content data in the field. The advantage of this method is the current PINNs framework does not need initial and boundary conditions and any information about the HCF a priori. The current framework must be tested with real experimental data for homogeneous soil in future research.

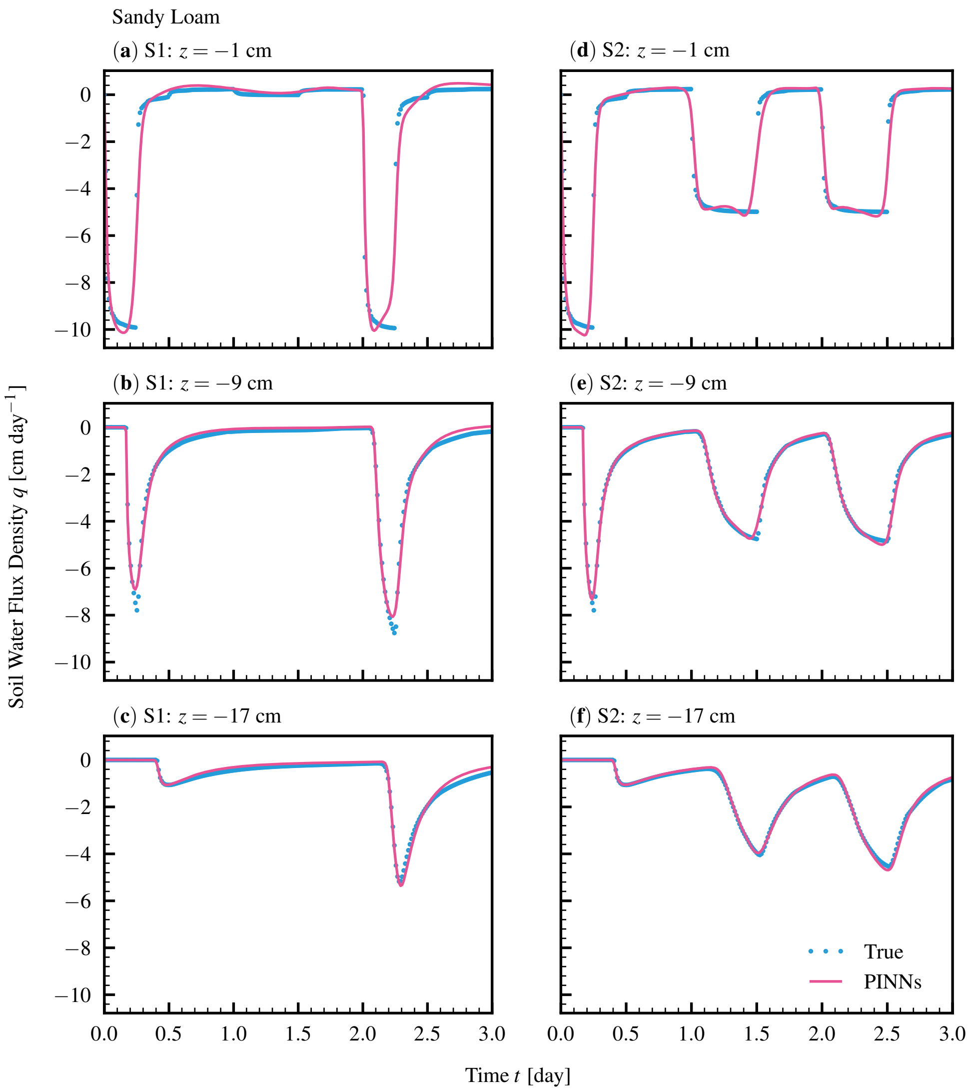

Figure 9: Estimated soil water flux density against the true one at three different depths for sandy loam soil. Scenario 1 (S1): (**a**) $z = -1$ cm, (**b**) $z = -9$ cm, and (**c**) $z = -17$ cm. Scenario 2 (S2): (**d**) $z = -1$ cm, (**e**) $z = -9$ cm, and (**f**) $z = -17$ cm.

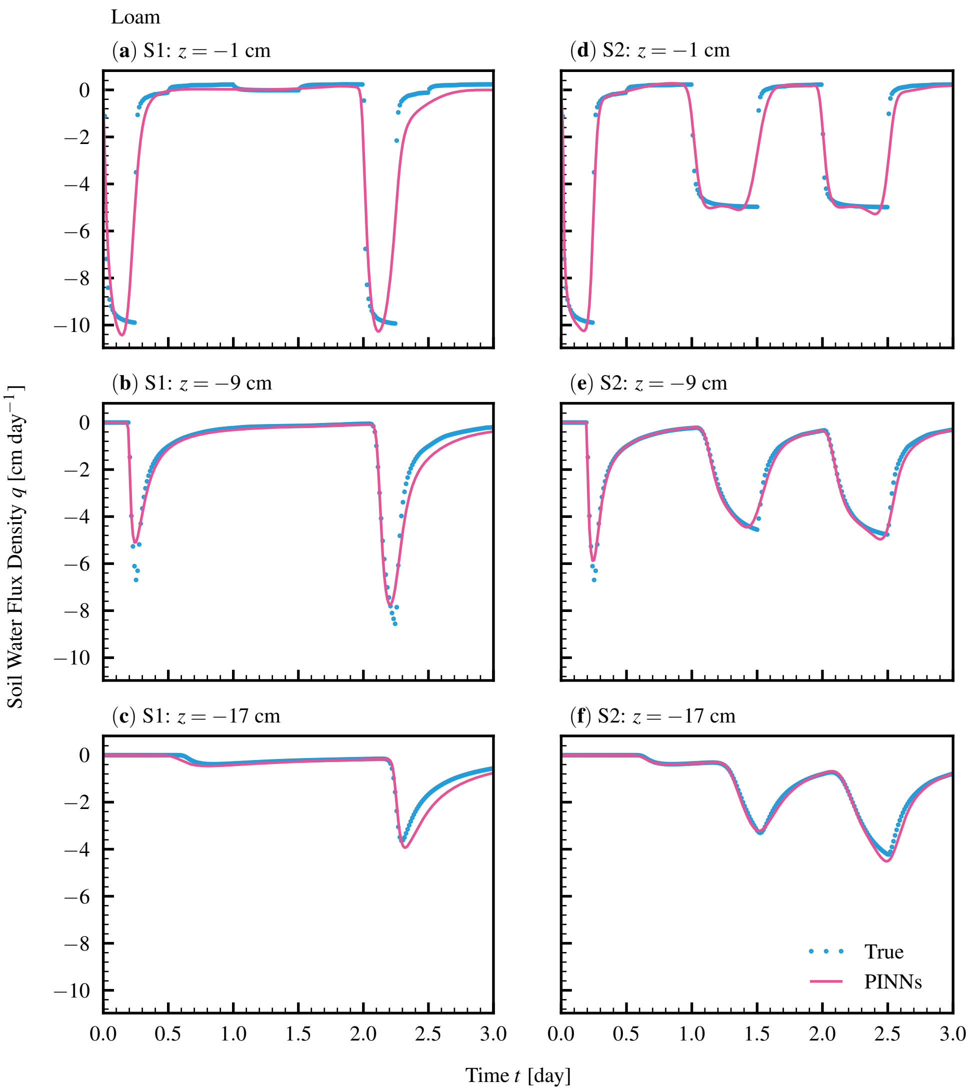

Figure 10: Estimated soil water flux density against the true one at three different depths for loam soil. Scenario 1 (S1): (**a**) $z = -1$ cm, (**b**) $z = -9$ cm, and (**c**) $z = -17$ cm. Scenario 2 (S2): (**d**) $z = -1$ cm, (**e**) $z = -9$ cm, and (**f**) $z = -17$ cm.

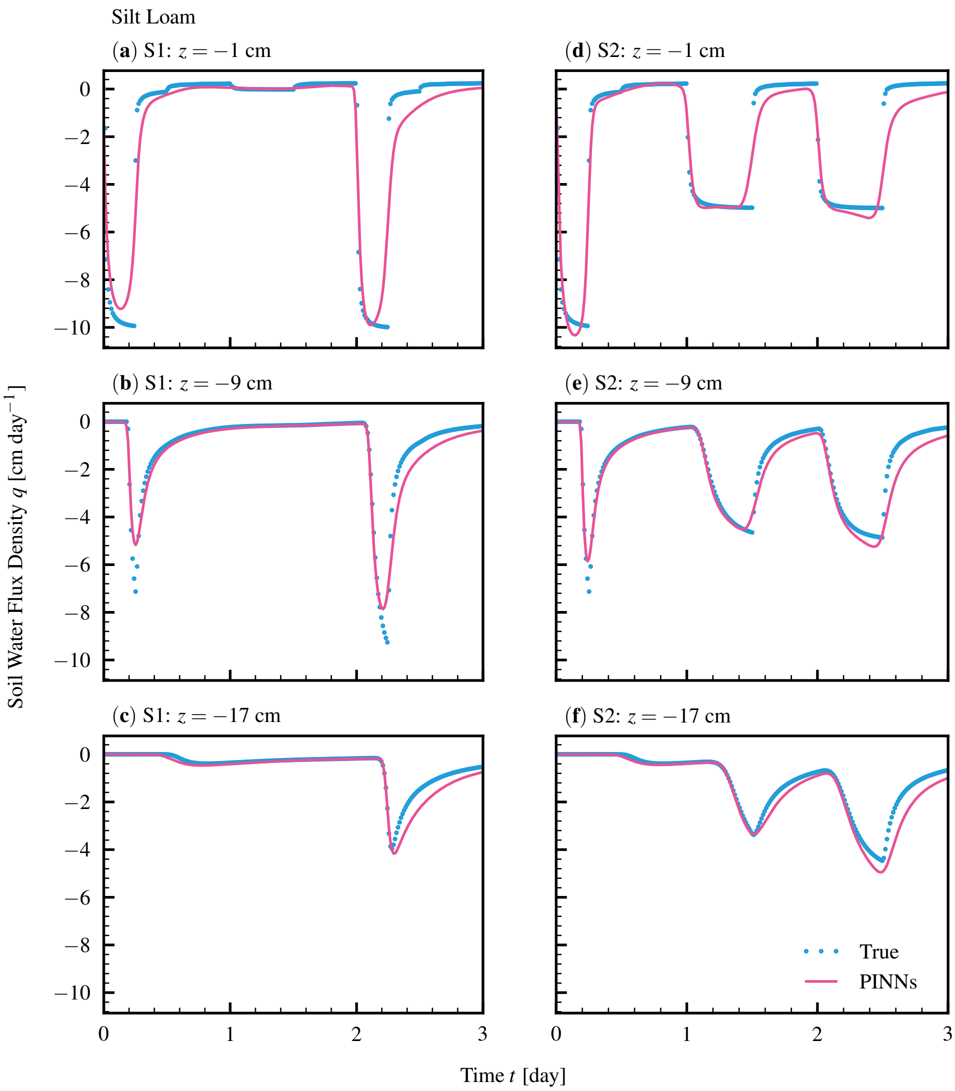

Figure 11: Estimated soil water flux density against the true one at three different depths for silt loam soil. Scenario 1 (S1): (**a**) $z = -1$ cm, (**b**) $z = -9$ cm, and (**c**) $z = -17$ cm. Scenario 2 (S2): (**d**) $z = -1$ cm, (**e**) $z = -9$ cm, and (**f**) $z = -17$ cm.

Acronyms

HCF Hydraulic Conductivity Function
PDE Partial Differential Equation
PINNs Physics-Informed Neural Networks
RRE Richardson-Richards Equation
WRC Water Retention Curve

Notation

:= Equal by definition
ˆ Hat indicating predicted values or functions (e.g., $\hat{y}$)
$^{(i)}$ Superscript (i) denoting ith data (e.g., $\theta^{(i)}$)
$^{[L]}$ Superscript [L] denoting Lth layer
$\mathbf{a}^{[L]} \in \mathbb{R}^{n^{[L]}}$ Vector value for the Lth layer consisting of $n^{[L]}$ units
$\boldsymbol{b}$ Bias vector
$\boldsymbol{g}$ Activation function
$\boldsymbol{h}$ Output function
$\boldsymbol{K}$ Hydraulic conductivity [L T^{-1}]
$\boldsymbol{K_s}$ Mualem-van Genuchen parameter
$\boldsymbol{\mathcal{L}}$ Loss function
$\boldsymbol{l}$ Mualem-van Genuchen parameter
$\boldsymbol{N}$ Number of data points
$\boldsymbol{n}$ Mualem-van Genuchen parameter
$\boldsymbol{q}$ Soil water flux density [L T^{-1}]
$\boldsymbol{\hat{r}}$ Residual of the Richardson-Richards euqation
$\boldsymbol{S_e}$ Effective saturation
$\boldsymbol{t}$ Time [T]
$\boldsymbol{W}$ Weight matrix
$\mathbf{x} \in \mathbb{R}^{n_x}$ Input vector for the size of the input n_x
$\mathbf{y} \in \mathbb{R}^{n_y}$ Output vector for the size of the output n_y
$\boldsymbol{z}$ Vertical coordinate (positive upward) [L]
$\boldsymbol{\alpha}$ Mualem-van Genuchen parameter
$\boldsymbol{\theta}$ Volumetric water content [L^3 L^{-3}]
$\boldsymbol{\theta_r}$ Mualem-van Genuchen parameter
$\boldsymbol{\theta_s}$ Mualem-van Genuchen parameter
$\boldsymbol{\psi}$ Matric potential of water in the soil [L]
$\boldsymbol{\psi_{log}}$ Matric potential in logarithmic scale

Acknowledgments

The publicly available code for physics-informed neural networks provided by Dr. Maziar Raissi (University of Colorado Boulder) was instrumental in the development of our model. The source code used in this study will be available online (the link added when the final version of the manuscript is ready).

References

Abadi, M., Agarwal, A., Barham, P., Brevdo, E., Chen, Z., Citro, C., ... Zheng, X. (2015). *TensorFlow: Large-scale machine learning on heterogeneous distributed systems.* Retrieved from `https://www.tensorflow.org/`

Babaeian, E., Sadeghi, M., Jones, S. B., Montzka, C., Vereecken, H., & Tuller, M. (2019). Ground, proximal, and satellite remote sensing of soil moisture. *Reviews of Geophysics*, *57*, 530–616. doi: 10.1029/2018RG000618

Bitterlich, S., Durner, W., Iden, S. C., & Knabner, P. (2004). Inverse estimation of the unsaturated soil hydraulic properties from column outflow experiments using free-form parameterizations. *Vadose Zone Journal*, *3*, 971–981. doi: 10.2113/3.3.971

Brooks, R. H., & Corey, A. T. (1964). *Hydraulic properties of porous media.* Fort Collins, CO, USA.

Buckingham, E. (1907). *Studies on the movement of soil moisture* (Vol. 38). Washington, DC, USA.

Byrd, R. H., Lu, P., Nocedal, J., & Zhu, C. (1995). A limited memory algorithm for bound constrained optimization. *Journal of Scientific Computing*, *16*(5), 1190–1208. doi: 10.1137/0916069

Cybenko, G. (1989). Approximation by superpositions of a sigmoidal function. *Mathematics of Control Signals Systems*, *2*, 303–314. doi: 10.1007/BF02836480

Daniels, H., & Velikova, M. (2010). Monotone and partially monotone neural networks. *IEEE Transactions on Neural Networks*, *21*(6), 906–917. doi: 10.1109/TNN.2010.2044803

Degré, A., van der Ploeg, M. J., Caldwell, T., & Gooren, H. P. A. (2017). Comparison of soil water potential sensors: A drying experiment. *Vadose Zone Journal*, *16*(4), 1–8. doi: 10.2136/vzj2016.08.0067

Durner, W. (1994). Hydraulic conductivity estimation for soils with heterogeneous pore structure. *Water Resources Research*, *30*(2), 211–223. doi: 10.1029/93WR02676

Durner, W., Jansen, U., & Iden, S. C. (2008). Effective hydraulic properties of layered soils at the lysimeter scale determined by inverse modelling. *European Journal of Soil Science*, *59*, 114–124. doi: 10.1111/j.1365-2389.2007.00972.x

Farthing, M. W., & Ogden, F. L. (2017). Numerical solution of Richards' equation: A review of advances and challenges. *Soil Science Society of America Journal*, *81*, 1257–1269. doi: 10.2136/sssaj2017.02.0058

Goodfellow, I., Bengio, Y., & Courville, A. (2016). *Deep learning.* Cambridge, MA, USA: The MIT Press.

Hopmans, J. W., Šimůnek, J., Romano, N., & Durner, W. (2002). Simultaneous determination of water transmission and retention properties. Inverse methods. In J. H. Dane & G. C. Topp (Eds.), *Methods of soil analysis, part 4, physical methods* (pp. 963–1008). Madison, WI, USA: Soil Science Society of America.

Iden, S. C., & Durner, W. (2007). Free-form estimation of the unsaturated soil hydraulic properties by inverse modeling using global optimization. *Water Resources Research*, *43*, 1–12. doi: 10.1029/2006WR005845

Kamai, T., Tuli, A., Kluitenberg, G. J., & Hopmans, J. W. (2008). Soil water flux density measurements near 1 cm d1 using an improved heat pulse probe design. *Water Resources Research*, *44*, 1–12. doi: 10.1029/2008wr007036

Kamai, T., Tuli, A., Kluitenberg, G. J., & Hopmans, J. W. (2010). Correction to "Soil water flux density measurements near 1 cm d1 using an improved heat pulse probe design". *Water Resources Research*, *46*, 1–5. doi: 10.1029/2010WR009423

Kingma, D. P., & Ba, J. B. (2014). Adam: A method for stochastic optimization. *arXiv preprint*, 1–15. Retrieved from `https://arxiv.org/pdf/1412.6980.pdf`

Kosugi, K. (1996). Lognormal distribution model for unsaturated soil hydraulic properties. *Water Resources Research*, *32*(9), 2697–2703. doi: 10.1029/96WR01776

Mualem, Y. (1976). A new model for predicting the hydraulic conductivity of unsaturated porous media. *Water Resources Research*, *12*(3), 513–522. doi: 10.1029/WR012i003p00513

Nocedal, J., & Wright, S. J. (2006). *Numerical optimization.* New York, NY, USA: Springer. doi: 10.1007/978-0-387-40065-5

Rai, P. K., & Tripathi, S. (2019). Gaussian process for estimating parameters of partial differential equations and its application to the Richards equation. *Stochastic Environmental Research and Risk Assessment*, *33*, 1629–1649. doi: 10.1007/s00477-019-01709-8

Raissi, M., & Karniadakis, G. E. (2018). Hidden physics models: Machine learning of nonlinear partial differential equations. *Journal of Computational Physics*, *357*, 125–141. doi: 10.1016/j.jcp.2017.11.039

Raissi, M., Perdikaris, P., & Karniadakis, G. E. (2019). Physics-informed neural networks: A deep learning framework for solving forward and inverse problems involving nonlinear partial differential equations. *Journal of Computational Physics*, *378*, 686–707. doi: 10.1016/j.jcp.2018.10.045

Richards, L. A. (1931). Capillary conduction of liquids through porous mediums. *Physics*, *1*, 318–333. doi: 10.1063/1.1745010

Richardson, L. F. (1922). *Weather prediction by numerical process.* Cambridge, United Kingdom: Cambridge University Press.

Robinson, D. A., Campbell, C. S., Hopmans, J. W., Hornbuckle, B. K., Jones, S. B., Knight, R., ... Wendroth, O. (2008). Soil moisture measurement for ecological and hydrological watershed-scale observatories: A review. *Vadose Zone Journal*, *7*, 358–389. doi: 10.2136/vzj2007.0143

Sheng, W., Zhou, R., Sadeghi, M., Babaeian, E., Robinson, D. A., Tuller, M., & Jones, S. B. (2017). A TDR array probe for monitoring near-surface soil moisture distribution. *Vadose Zone Journal*, *16*(4), 1–8. doi: 10.2136/vzj2016.11.0112

Šimůnek, J., Šejna, M., Saito, H., Sakai, M., & van Genuchten, M. T. (2013). *The HYDRUS-1D software package for simulating the one-dimensional movement of water, heat, and multiple solutes in variably saturated media, Version 4.17* (Tech. Rep.). Riverside, CA, USA: Department of Environmental Sciences, University of California Riverside, Riverside.

Skierucha, W. (2000). Accuracy of soil moisture measurement by TDR technique. *International Agrophysics*, *14*, 417–426.

Tartakovsky, A., Marrero, C. O., Perdikaris, P., Tartakovsky, G. D., & Barajas-Solano, D. (2018). Learning parameters and constitutive relationships with physics informed deep neural networks. *arXiv preprint*. Retrieved from `http://arxiv.org/abs/1808.03398`

van Genuchten, M. T. (1980). A closed-form equation for predicting the hydraulic conductivity of unsaturated soils. *Soil Science Society of America*, *44*, 892–898. doi: 10.1016/j.pan.2017.07.214

Wang, S., Teng, Y., & Perdikaris, P. (2020). Understanding and mitigating gradient pathologies in physics-informed neural networks. *arXiv preprint*. Retrieved from `https://arxiv.org/pdf/2001.04536v1.pdf`

Zha, Y., Yang, J., Zeng, J., Tso, C. M., Zeng, W., & Shi, L. (2019). Review of numerical solution of Richardson–Richards equation for variably saturated flow in soils. *Wiley Interdisciplinary Reviews: Water*, *6*, 1–23. doi: 10.1002/wat2.1364